

MINERvA neutrino detector response measured with test beam data

MINERvA Collaboration

MINERvA Addresses placeholder in template

Abstract

The MINERvA collaboration operated a MINERvA-like solid scintillator sampling calorimeter in a hadron test beam at the Fermilab Test Beam Facility. This article reports measurements with samples of protons, pions, and electrons from 0.35 to 2.0 GeV/c momentum. Overall the MC describes the data within 3 to 4%, though some features of the data are not perfectly modeled by a Monte Carlo simulation of the experiment and particle interactions from Geant4. From these data, calibrations of Birks' constant, calorimetry, and a test of proton tracking efficiency are also obtained. These results are used to tune the MINERvA detector simulation and evaluate systematic uncertainties in support of the MINERvA neutrino cross section measurement program.

Keywords: hadron calorimetry, electromagnetic calorimetry, Birks' Law, test beam

PACS: 13.75.-n 13.75.Cs 29.40.Vj

Note to MINERvA reviewers

This list will allow for quick location of additional information and supporting plots from our tech notes, and will be removed before being submitted to NIM.

- 5 Test beam beamline resolution and systematic errors
 - Devan and Gran, TN017, docdb:8547
 - Test beam detector calibrations, Gran et al., TN018 docdb:8686
 - Pion reaction cross section, Higuera, TN033 docdb:9031
 - Birks' law parameter from MINERvA testbeam data, Gran, TN037 docdb:9131
- 10 Test beam pion calorimetry, Gran, TN045 docdb:9474
 - Electron calorimetry and the e/π ratio, Bergan, docdb:9929
 - Test beam proton calorimetry, Devan, TN051 docdb:9986
 - Short track reconstruction efficiencies using test beam protons,
McGivern, TN048, docdb:10367

15 1. Introduction and test beam goals

The MINERvA experiment[1] is designed to make measurements of neutrino nucleus cross sections with high precision. An important part of these [2, 3, 4, 5, 6] and future cross section measurements is the estimate of the energy of one or more hadrons exiting the nucleus. These are moderate energy recoil nucleons (especially protons) with energy from hundreds of MeV to a few GeV, pions from inelastic production, plus softer nucleons and nuclear fragments. The goal of the test beam experiment is to validate the Monte Carlo simulation of the detector response to these particles. Results presented in this paper include a measurement of the Birks' law parameter, constraints on the accuracy of proton, pion, and electron calorimetry, and a study of tracking efficiency for protons.

The detector used to take these data is identical in most respects to the MINERvA detector installed in the NuMI neutrino beam at Fermilab, but in miniature. These test beam data are the first from a new hadron beamline at the Fermilab Test Beam Facility (FTBF) for a data run in summer 2010 as Fermilab Test Beam Experiment T977. There are differences between the two detectors that mitigate special aspects of the beam environment in FTBF and allow for a data set better focused on the Birks and calorimetry results.

The energy range covered by these data is well matched to the energy range of protons and pions and electromagnetic showers in the 2010 to 2012 MINERvA low energy neutrino and anti-neutrino data. This is especially true for the reactions from neutrino quasi-elastic scattering through Δ and other resonance production. Measuring differential cross sections for these exclusive final states is a pillar of the MINERvA neutrino physics program. These energies also cover the lower part of the range expected for hadrons produced in neutrino deep inelastic scattering.

The material in this paper starts with a description of the testbeam, then the detector, and the resulting data sample with its simulation and calibrations. The Birks' Law parameter measurement is next because it the best value for the parameter is used for all other analyses. Proton calorimetry results are

presented followed by a section with a complete discussion of systematics for both proton and pion measurements, which share the same sources but take on different values. With the systematics discussion as a prelude, the pion calorimetry results are described, followed by the the electron calorimetry results, and then a summary discussion of calorimetry in general. A constraint on tracking efficiency rounds out the material and is followed by a conclusion.

2. Fermilab Test Beam Facility tertiary hadron beam

This beam is available because of a partnership between the MINERvA experiment and the Fermilab Test Beam Facility. It is produced from 16 GeV pions colliding with a copper target. All species exit a collimator with an angle of 16 ± 1 degrees from the direction of the incident pions. The species and momentum are tagged particle-by-particle using time of flight (TOF) and position measurements from four wire chambers. Fig. 1 shows the geometry and coordinate system viewed from the top with the beam propagating left to right where it first encounters the target and collimator. Two magnets each carry

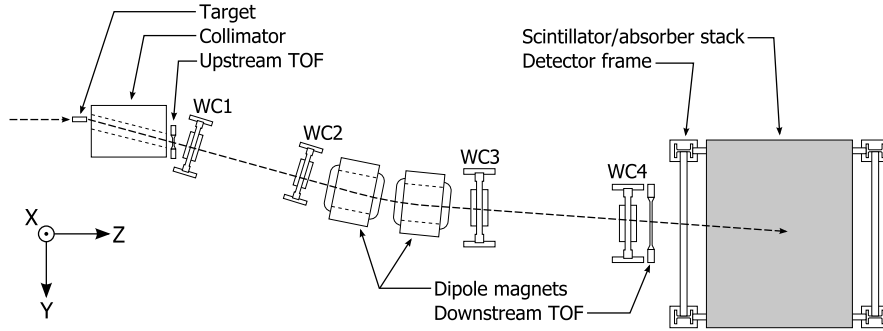


Figure 1: Diagram of the beamline built for this experiment, viewed from above with the beam going from left to right.

100 A of current and the polarity can be reversed. The typical field integral is 38.3 Tesla cm with 1.5 Tesla cm variations around this value that encompass

90% of selected events. The detector on the right sees a range of incident particles with low momentum at low Y-coordinates and normal incidence and high momentum at higher Y-coordinates and with angles as high as 10 degrees with
65 respect to the detector Z-axis.

With the 1.07 m wide detector aperture and our chosen beam tune, the beam delivers a broad distribution of protons and pions from 0.35 to 3.0 GeV/c momentum. The usable momentum range for these analyses is 0.35 to 2.0 GeV/c which provides proton, π^+ , and π^- samples each with roughly ten thousand particles. This is enough that these measurements are systematics dominated. The
70 electron content of the beam is small and limited to momenta below 0.5 GeV/c, but has enough events for analysis. In addition, there is a 5% component of kaons, plus smaller components of deuterons and alpha particles which are not part of the results presented here.

75 The pion, kaon, proton, and deuteron/alpha components are well separated, shown in Fig. 2 after quality cuts. Low momentum electrons barely discernable near 20 ns in this figure. There is also an accidental background near 39 ns when another particle coincidentally passes through the TOF. This happens because the Fermilab Main Injector Accelerator supplying the beam has a 53 MHz time
80 structure where pions striking the copper target are likely separated by integer multiples of 19 ns .

The separation shown in Fig. 2 allows species to be selected based on momentum, TOF, or the combination of the two plus the measured pathlength that gives an estimator for the mass of the particle. Protons (and kaons) are
85 selected by requiring the mass lies within $\pm 20\%$ of the true mass of the particle. The selection is wider for pions and based on TOF because the TOF resolution is the limiting factor and we do not cut events just because their TOF measurement fluctuates to super-luminal. So the lower bound is based on a range near the expected TOF of a pion, the upper end is based on the TOF for the pion
90 mass plus 20% plus an extra 5 ns. The purity of the pion and proton selection is better than 99%, estimated by extrapolating the tails of the wrong-species distribution under the selected events. An electron selection is more complex

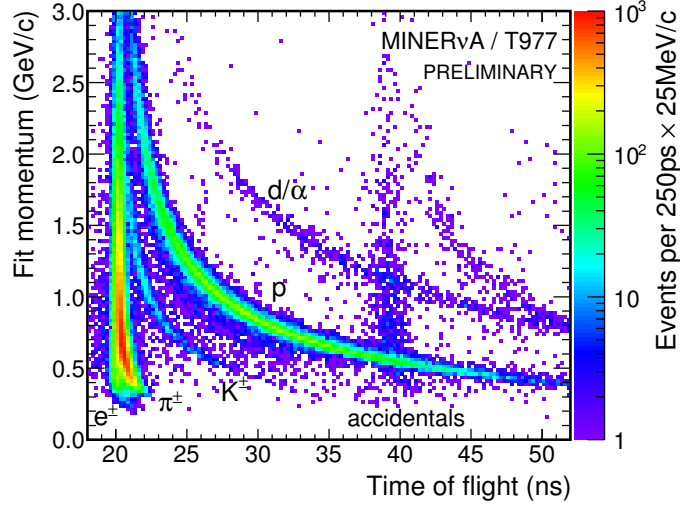


Figure 2: The measured momentum and time of flight used to separate different particle species and backgrounds.

and includes pion rejection criteria, and described in Sec. 9.

The momentum estimate is accurate to 1% at low energy and 2% at high
 95 energy. It uses a detailed map of the magnetic field calculated for us using finite
 element analysis software from the specifications for the two dipole magnet coils
 and steel and the position survey of their placement relative to each other. The
 central value of the magnetic field from the calculation is adjusted down 0.58%
 to match the actual field of the magnet from in-situ measurements. Longitude
 100 and transverse measurements of the field were taken with the magnets installed
 in their final positions. These measurements are well described by the calcu-
 lated field. How accurately they are modeled is one basis for estimating the
 uncertainty in the momentum. The other uncertainty comes from the accuracy
 of the position survey of the four wire chambers.

105 The momentum resolution is also evaluated particle-by-particle and is 2.5%
 for pions and ranges from 5% to 3% for low to high momentum protons. It
 is driven by multiple scattering and non-uniform magnetic field effects at low
 momenta and by the wire pitch and beamline length at high momenta. The

iterative momentum fit uses a stepper within the non-uniform calculated field
 110 to estimate the field integral, then a Kalman Filter technique is used to obtain
 the momentum and its uncertainty for each trigger. The resolution of the mo-
 mentum estimate is modeled accurately enough and is not a limiting factor for
 these analyses. The 200 ps resolution of the time of flight system limits the
 ability to separate electrons from pions. This TOF resolution is a source of
 115 uncertainty for those calorimetry results.

3. MINERvA test beam detector and calibration

The detector exposed to this FTBF beam (hereafter called the test beam
 detector) is a miniature version of the MINERvA detector installed in the NuMI
 neutrino beam [1] (hereafter called the MINERvA detector). It is made of 40
 120 square planes of 63 nested triangle shaped scintillator strips each with length
 107 cm and thickness 1.7 cm. This contrasts to the MINERvA detector which
 has a hexagon shape made of 124 planes of 127 strips in the central tracker
 region followed by another 20 planes each of ECAL and HCAL with Pb and
 Fe interleaved respectively. Both detectors share the same three-view UXVX
 125 sequence of planes with U and V rotated ± 60 degrees relative to the X plane that
 defines (for the testbeam detector) the vertical coordinate system. This allows
 for dual stereo reconstruction of multiple tracks for the MINERvA detector and
 very good reconstruction of single tracks in the test beam detector.

The readout chain from scintillator to wavelength shifting (WLS) fiber to
 130 photomultiplier tube (PMT) to digitization is almost identical. The exception is
 the test beam detector has no clear fiber optical cables; the WLS fiber connects
 directly to the PMT a half-meter out of the plane. The effect of smaller scin-
 tillator planes and no clear fiber is that the test beam detector has about 50%
 higher light yield for a given energy deposit, and corresponding better resolution
 135 for some kinds of measurements, compared to the MINERvA detector.

Unlike the MINERvA detector which has the PMT assemblies for every plane
 on the same side, the test beam detector alternates them in groups of four planes,

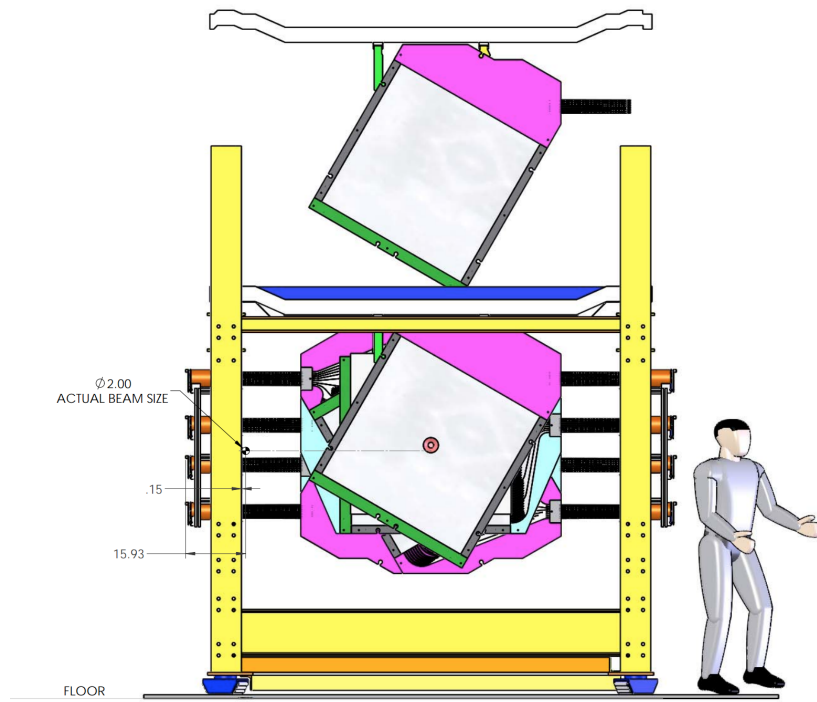


Figure 3: An engineering drawing of the detector viewed from the front. The third U plane is being lowered onto the stand behind eight installed planes. Drawing also illustrates the every other side readout in sets of four. If this was the ECAL, there would be a plane of Pb absorber inbetween each plane.

one UXVX set rotated 180 degrees. Mechanically this allows the planes to be placed closer together than the frames and PMT assemblies would otherwise permit. The result is an air gap only slightly larger than in the MINERvA detector. Because the beam bend magnets steer different momentum particles to different portions of the detector (and at different angles) there is a correlation between the geometry and the position dependent optical attenuation of the readout. Alternating the readout mitigates a few-percent momentum dependent uncertainty, making this effect negligible.

The detector energy scale is calibrated using the same strategy as the MINERvA detector installed in the NuMI neutrino beam, and is described in [1]. An initial estimate for photoelectron yield is obtained for each strip using standard pedestal and gain measurements. The intrinsic differences in response between strips are analyzed to produce a correction factor to make the response from strip to strip uniform. As a side effect, these muons also gives geometric plane position corrections. Then the absolute energy scale is done using a muon equivalent unit technique. This ensures the peak number of photoelectrons at the PMT is the same in the data and simulation. Then the simulated geometry and Geant4 energy loss are used to set the absolute energy scale.

One difference with the MINERvA detector is the muon equivalent unit absolute response calibration is carried out with broad spectrum cosmic ray muons (and a simulated spectrum with the same angular distribution) rather than momentum-analyzed muons from the NuMI beam. These calibrations do not include energy that appears off the muon track due to cross talk, a feature treated separately in the analyses described in this paper. The calibration uses the peak of the dE/plane response for muons, and depends little on muon δ -ray and bremsstrahlung production in the tail of that distribution.

In addition, temperature dependence is more important than it is in the NuMI hall. The detector hall warmed during the day and cooled at night, so the overnight cosmic muon sample spans the same range of temperature as the daytime hadron sample. The detector response is corrected for that temperature dependence and a residual uncertainty is included with the systematic

uncertainties.

170 Unlike the MINERvA detector, the test beam detector's removable absorber planes allow for exposures of two configurations. One has 20 planes with 1.99 mm thick Pb absorber (ECAL) followed by 20 planes with 26.0 mm thick Fe absorber (HCAL). The absorber is interleaved by placing one absorber upstream of each scintillator plane. The other has 20 planes with no absorber (tracker)
175 followed by 20 planes of ECAL. For compactness, this document will refer to these configurations as EH and TE, respectively. To illustrate, in Fig. 3, the first nine planes of the TE are shown with no absorber, but starting before the 20th plane, another hanger with a sheet of Pb would be lowered before each succeeding scintillator plane. For the EH configuration, a hanger holding a Pb
180 sheet is installed before the first U plane and for all the first 20 planes, then a hanger with an Fe plate is installed in front of each of the remaining 20 planes. This replicates the main downstream regions of the MINERvA detector, which has 124 planes of tracker followed by 20 planes of ECAL and 20 planes of HCAL.

4. Data sample and simulation

185 The selected data samples with the matching simulated spectra are illustrated in Fig. 4. There are plots of the energy spectra for protons in both detector configurations and π^+ , π^- in the EH configuration. At these momenta, pions leave the back of the TE detector and are not used for a calorimetric analysis. The data samples are selected using the momentum and time of flight measurements shown in Fig. 2 usually expressed simply as the reconstructed mass of
190 the particle, plus selections to ensure a quality measurement as a particle passes through the beamline instrumentation and into the detector.

In this analysis, the data are compared to a full, high statistics Monte Carlo simulation (MC). The spectrum for the simulation are generated from the actual data particles' position and momentum measured at the third wire chamber,
195 with momentum and angle smeared according to the estimated resolution on a particle-by-particle basis. The simulation then propagates particles through the

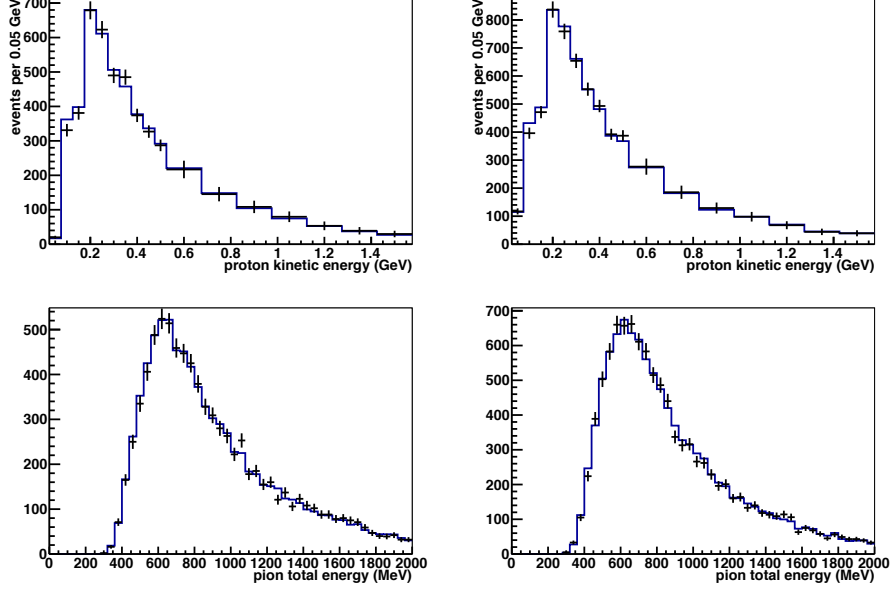


Figure 4: Measured spectra for proton EH (top left), proton TE (top right), π^+ EH (bottom left), π^- EH (bottom right) samples, after selection. The blue histogram is taken from a Monte Carlo simulation that was seeded with measured particle momenta and trajectories from the data, so by construction the spectra are the same.

material of third and fourth wire chamber, the downstream TOF, the cosmic
muon trigger scintillator, the air, and finally into the detector. Using the esti-
200 mated energy and position resolution for each particle and a Gaussian random
smearing allows us to use the same data particles multiple times and generate
large MC samples, typically 20 to 40 times larger than the data. We observe
that the MC reproduces the data for the special situations where the beamline
energy resolution dominates, such as for protons that stop at the end of their
205 expected range, validating that the beamline characteristics are well simulated.

The MC does not simulate any beamline induced background effects, nei-
ther from particles that are exactly in-time (from the same parent 16 GeV pion
hitting the target) nor secondaries from another pion in an nearby 19 ns slot in
the Fermilab Main Injector 53 MHz accelerator structure. Because we collect

210 data for 16 microseconds around each trigger, and because some incident particles should spatially leave much of the detector quiet, the data itself contains a record of the average beam-induced background around valid triggers.

These effects were validated, and some cleaning selections were developed using the revolutionary web-based MINERvA event display [7], in many cases
215 with the help of undergraduate research assistants. The main selection requires the particle to appear in the detector at a location and time predicted by the measurement in the beamline, and not have substantial secondary activity consistent with a second particle (especially muons) passing through at nearby times. Events with additional reconstructed activity within 250 ns before and
220 500 ns after are also cut. These selections reduce both beam-induced backgrounds and also eliminate triggered particles that scattered substantially in the beamline before reaching the detector. The selections to reduce these unwanted events are applied to both the data and simulated samples. Finally, we estimate and make a statistical subtraction of the remaining background and
225 evaluate an uncertainty specific to each analysis.

The basis of the simulation uses Geant4 version 9.4p2 [8, 9] and our best description of the detector geometry and material [1]. The scintillator plane is made of 1.801 g/cm² of plastic scintillator, WLS fiber, and a co-extruded TiO₂ reflective coating. Added to this is another 0.226 g/cm² of epoxy and
230 Lexan. The scintillator planes were made at the same facilities immediately following the production of MINERvA planes, and the modifications for assembling smaller planes make negligible difference. The uncertainty on the amount of the material is the same 1.5% as for the MINERvA detector. In the ECAL portion of the detector there are planes of Pb with thickness 2.30 g/cm² and
235 in the HCAL version there is 20.4 g/cm² material that is 99% Fe and 1% Mn. The Pb and Fe absorber are similar to the MINERvA detector, but we use the as-measured test beam detector quantities in the simulation and to evaluate material assay uncertainties (coincidentally) of 1.2% for each.

Almost all aspects of the detector response are simulated using details con-
240 strained by calibration data and bench tests, including the temperature correc-

tion described previously and the Birks' law parameter measured from these data, described in next in Sec. 5. Cross talk arises because each scintillator strip corresponds to a pixel in a 64 channel PMT, leading to optical and some electronic cross talk, which is simulated and tuned to data. A few features
245 are not simulated, of which PMT after-pulsing and PMT non-linearity are only significant for high pulse-height activity.

5. Birks' Law parameter

After calibration of the beam and detector, we measure the Birks' law parameter [10, 11] for the MINERvA polystyrene scintillator [1]. Birks' law describes
250 the quenching effect on scintillation photons produced by high, localized energy deposits. Its an important effect at the end of proton tracks in MINERvA, and affects calorimetry measurements both there and in this paper.

A sample of protons that clearly stop in the detector are selected from the entire proton TE sample, giving a large sample of protons at the end of their range.
255 Protons that appear to stop between planes 9 and 19 inclusive are checked that their range is consistent with their incoming energy. The energy dependence of the expected range in the detector is not determined using a simulation. For events that stop in a particular plane, the end-of-range protons form a peaked distribution at the appropriate kinetic energy while protons that interact are a
260 tail extending to higher energy. We select the former, and do so separately for both data and simulated events.

The proton range is very well modeled by the simulation. The simulated protons stop 1.1% earlier than the data, which is a smaller discrepancy than the 1% beamline momentum plus 1.4% material assay uncertainties. This cross-
265 check uses a Gaussian fit to find the end-of-range peak used to select the Birks' analysis sample, and is shown in Fig. 5. Stopping protons are such a high resolution sample, the widths of those Gaussian fits (10 to 15 MeV, not shown) are primarily driven by the beamline and multiple scattering resolutions, and are also well described by the simulation.

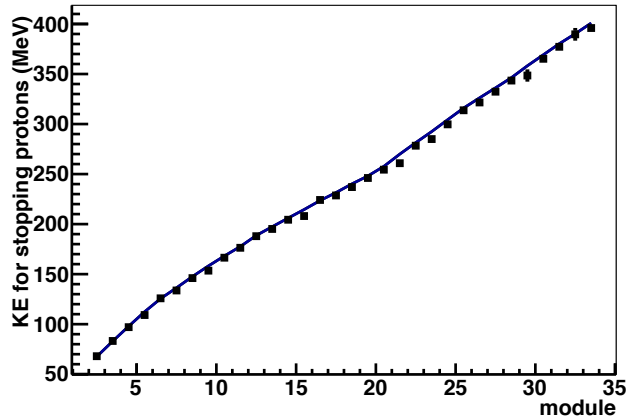


Figure 5: Kinetic energy from the mean of a Gaussian fit to the peak energy for protons that appear to stop in each TE plane (module). The MC stops 1.1% earlier than the data, a discrepancy which is smaller than the beamline momentum and material assay uncertainties. Most error bars are less than 1% and are too small to see.

Birks' empirical parameterization of the quenching factor to be applied to photons/MeV is

$$\text{Suppression factor} = \frac{dE}{1.0 + \text{Birks Parameter} \times (dE/dx)},$$

with one parameter, often abbreviated k_B with units of mm/MeV. This suppression is implemented in the MC as a suppression applied to MC deposits based on the ΔE and Δx as the simulation steps the particle through the active scintillator material. If the parameter k_B is too high, the MC will show a discrepancy of too much suppression in the energy per plane that increases toward the end of a proton's range, with the data having the higher energy response. The left plot in Fig. 6 shows such a trend using the default value of 0.133 ± 0.04 mm/MeV used by MINERvA until the present measurement. The mean energy loss is better described by a MC with the higher response (lower parameter value) as a function of the distance from the observed end of the proton's path into the detector, the top line.

The left plot, and the extraction of a better value for Birks' parameter is done

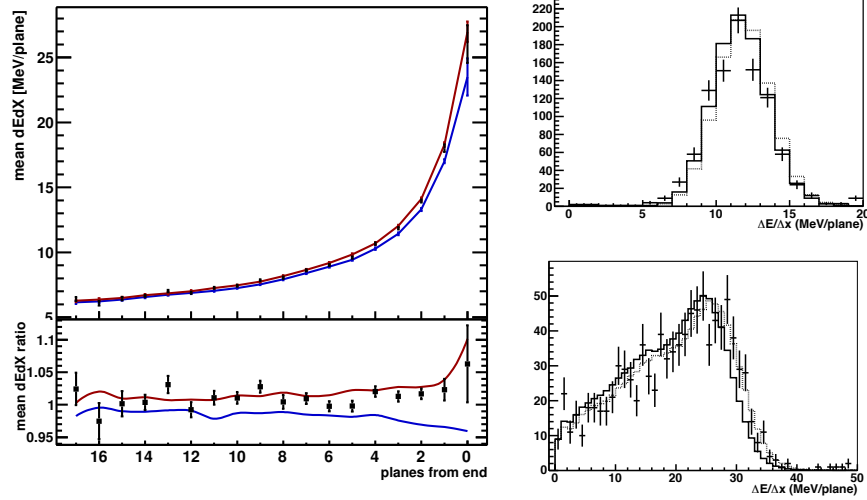


Figure 6: The measured energy deposit per plane for data compared to the simulation with the before-fit Birks' parameter of 0.133 mm/MeV and the original -30% (top line) and +30% (bottom line) uncertainty on this parameter's initial value. The figures on the right show the underlying binned energy per plane, *at best fit for the non-Gaussian end plane zero, and the more Gaussian plane three*. The MC distributions on the right show the smaller 17% uncertainty bounds, one shifted to higher values on the horizontal axis, one shifted lower, such that the best fit parameter (not shown) would lie between them in every bin, see discussion.

using binned data for the energy per plane. Two examples of the underlying data are shown on the right of Fig. 6, the top one for the plane three from the end, and one for the plane at the end (zero planes from the end). These two distributions are shown for the best fit with the (smaller) best fit uncertainty 0.0905 ± 0.015 mm/MeV, and are also being used here to illustrate how the fit is constructed.

The binned distribution is formed for all activity as a function of planes from the end of the proton's observed activity. Because protons stop different distances in the detector, the contents of any one distribution contain data from many physical planes. This technique is less sensitive to uncertainties in modeling the proton momentum, material assay, and detector response. Planes further from the end than the first fourteen have low statistics because only

a small fraction of the events contribute to them, and are excluded from the
 295 analysis. To support systematics studies, the analysis keeps only bins in the
 central region of each distribution to ensure they will remain populated when
 systematically shifted samples are constructed. In the example of plane three,
 bins from 6.0 to 15.0 MeV are included, while plane zero includes bins from
 10.0 to 32.0 MeV, making a total of 123 bins across the fourteen planes-from-
 300 end included in the analysis. Most planes of data can be well-fit with a Gaussian,
 which is used to make visualizations of the trend such as the left plot in Fig. 6.
 On the other hand, the activity in the plane at the end is especially non Gaussian
 because different protons stop different distances into that plane. As this plane
 is the one with the most sensitivity to Birks' parameter, the fit uses the binned
 305 distributions directly.

Birks' parameter is extracted iteratively. The original default value of the
 parameter and its uncertainty is used to make three full MC samples to ex-
 tract a new parameter and smaller uncertainty. As shown in Fig. 6, the MC
 samples with $\pm 1\sigma$ usually bracket the data. For a trial Birks' parameter, the
 310 predicted binned distribution is formed by interpolating between these two sam-
 ples, or when necessary extrapolating slightly beyond these samples. By scan-
 ning through a full range of parameters, the one that returns the lowest χ^2 is
 used to seed the next iteration of the analysis.

In the fit, the overall energy scale is an unconstrained parameter, which si-
 315 multaneously accounts for both the energy scale uncertainty and the correlation
 between the calibrated energy scale and Birks' parameter. Every iteration of
 the fit also scans over this parameter by applying a scale factor to each MC
 event and reforming each histogram. This causes individual entries in each
 binned histogram to shift upward or downward, equivalent to moving the mean
 320 of each distribution by the same amount, and allowing the fit to seek a better
 χ^2 minimum.

Also, an amount of dE smearing that accounts for unsimulated calibration
 effects was allowed to vary, though it yields the same 5.5% result [1] as found for
 the MINERvA detector. This was not done for every iteration, only for values

325 near the best fit result in the later iterations.

In summary, the best value is obtained using a parameter scan in this three parameter space of Birks' parameter, energy scale, and smearing of reconstructed energy deposits. The procedure is iterated with a new MC built from the new parameter value and smaller \pm shifted values; after three iteration
330 the procedure reliably converges to the final result.

The best value for the Birks' parameter is 0.0905 ± 0.014 mm/MeV. This value is near the -1σ limit of the original estimate used by MINERvA for analyses through 2014, confirming we use suitable Birks' effect uncertainties in prior publications. Future simulations using the new value have half the prior uncertainty. The best fit describes the data well, yielding a χ^2 of 124 for 120 degrees
335 of freedom. In addition to showing the method of the fit, the two right figures in Fig 6 show examples of the goodness of fit.

The measurement of the Birks' parameter is dominated by systematic uncertainties. One of the largest is from the correlation with the energy scale, which
340 is treated as an unconstrained parameter in the fit. The fit value is sensitive to variations of which protons, which physical planes, and which bins are included in the fit. Uncertainties in the material assay are propagated to the result using modified full MC samples. Extra smearing of the scintillator and PMT response to single energy deposits in the MC has a small effect. Two special sources of
345 uncertainty, the effect of Geant4 step size and of PMT nonlinearity are described below. All these effects are summarized in Tab. 1.

Because Birks' parameter is obtained by matching the MC simulation to data, it might be considered an effective parameter. In addition to energy scale correlations and Birks' quenching, it is accounting for the accuracy of the Geant4
350 energy loss simulation and our choice to use the default (adaptive) Geant4 step size. Allowing Geant4 to take more coarse steps, up to the scale of one scintillator bar per step, yields an increase in the simulated response of about 4% in the last plane and a slightly better $\chi^2 = 118$. The typical simulated Δx has increased, so $\Delta E/\Delta x$ has decreased, so there is less Birks' suppression applied. Such an extreme effect would cause a bias in the fit Birks' parameter of
355

Source	percent
hline from fit	-7 +5
proton selection	-11 +3
Geant4 step size	-0 +9
PMT nonlinearity	-3 +0
material assay	± 5
physical planes	± 5
MC energy smearing	± 3
choice of bins	+3 -0
Total	+16% -13%

Table 1: Percent systematic uncertainties on the value for Birks' parameter from different sources.

0.008, about half the total uncertainty. However, this particular measurement is specifically matched to the Geant4 and hit aggregator settings that are used by the MINERvA simulation as of late 2014. This uncertainty should be included when comparing to other measurements but is not an uncertainty on the
360 resulting simulation used for MINERvA neutrino analysis.

Another detector response parameter that has systematic effects, especially on calorimetry but only a little here, is the nonlinear response of the photomultiplier tubes due to saturation effects in the dynode current. This nonlinearity sets in for high instantaneous current at the anode, and so is a function
365 of charge measured by the front end board's digitization module. As of this writing, MINERvA does not have an in-situ measurement under circumstances that are equivalent to the light propagating in our scintillator bars and WLS fiber. Instead, we have a reference non-linearity curve obtained from bench tests. The dE/plane profile in Fig. 6 is distorted by nonlinearity in ways different from
370 either Birks' parameter or energy scale, so we investigate the size of possible nonlinearity. Applying non-linearity of 20% of the reference degrades the χ^2 by one unit, with a correlated shift in Birks' parameter. Thus at 25 MeV per

plane (rightmost point in Fig. 6) we do not have sensitivity to nonlinearity effects with these data. We use this 20% to get an uncertainty for the Birks' parameter measurement. An ab-initio upper bound of 50% of the reference accounts for the translation of the bench measurement to the real detector situation. That larger bound is used later for calorimetry to account for non-linearity effects when higher energies are deposited in a single strip.

These results are consistent with other values for the Birks' quenching parameter. A recent review of the properties of many materials including polystyrene is available in [12] with references and one additional later measurement [13]. The parameter value is expected to depend primarily on material formulation. These measurements are focused on heavily ionizing nuclear fragments and alpha particles which are important in dark matter and double beta decay experiments as well as nuclear fission studies. The technique is conceptually similar to using the end of a proton track but potentially more sensitive due to the enhanced ionization and granularity of the data. The analysis of [12] obtains a value of $0.0090 \text{ g / cm}^2 \text{ MeV}$ (with no uncertainty given) for polystyrene based scintillator. Using the 1.06 g/cm^3 density of polystyrene quoted in that analysis, this converts to 0.085 mm/MeV . This value and the Birks' parameter result above for our scintillator formulation and density of 1.043 g/cm^3 are nearly identical.

6. Proton calorimetry

This test beam experiment is designed to constrain the uncertainty on the single particle calorimetric response to protons and pions. For low multiplicity neutrino events we reconstruct the hadron response particle-by-particle using range, calorimetry, or a combination of the two. For high multiplicity hadron systems from neutrino events, the total energy of the hadronic recoil system (everything but the outgoing charged lepton) is calorimetrically reconstructed. When the hadron(s) interact in the detector, energy is spent unbinding nucleons from nuclei and other energy goes to neutral particles. An estimate of this missing energy is used to correct the observed response and obtain an unbiased

estimator for the hadron system. In all cases, a major ingredient is the MC prediction for the single particle response, which is constrained with these data.

The hadron event is reconstructed by summing the calibrated energy measured in the scintillator. The standard tracking algorithm is applied to each event. If a track segment is found, the 3D location of hits on the track are known and used to make a correction for attenuation in the scintillator strip to the point where the particle passed. For all hits not on tracks, the attenuation estimate is made to the center of the strip. Then a correction for the passive material fraction for each plane is applied; a factor of 1.255 in the tracker, 2.077 in the ECAL, and 10.727 in the HCAL. Cross talk is not included when the muon equivalent technique is used to set the energy scale, but is measured as a byproduct of that calibration. Because cross talk is proportional to the total of the energy deposits, the measured cross talk fraction of 4.2% is subtracted from both data and MC.

The activity recorded over the 150 ns digitization time is summed into the response, unlike the typical MINERvA neutrino analysis which uses a window from -20 ns to +35 ns around the peak in the cluster timing distribution. Activity later than 150 ns from low energy neutrons and decay electrons is not included. The former is predicted to amount to a few percent of the available energy and appears in the detector over several microseconds.

For the proton calorimetry analysis, the beamline induced backgrounds are reduced using additional selections. For the lowest proton energies, below 0.15 GeV for TE and 0.2 GeV for EH, the back half of the detector is not included calorimetrically at all and is used as a muon/pion veto by rejecting events with greater than 10 MeV of activity. Up to 0.3 GeV (TE) or 0.7 GeV (EH), backgrounds are reduced by using a 2 MeV threshold for activity in the last four planes to veto background activity from the beam. At the highest energies, there is no background subtraction.

The resulting corrected estimate for the energy is compared to the available energy, which is just the kinetic energy for the proton. The distribution of this fractional response is the primary measurement and is calculated event-by-

event. Then the events are binned by incident particle energy, from which we compute the mean and RMS for each bin. The results for the mean are plotted in Fig. 7. The error band on the MC represents the total systematic uncertainty.

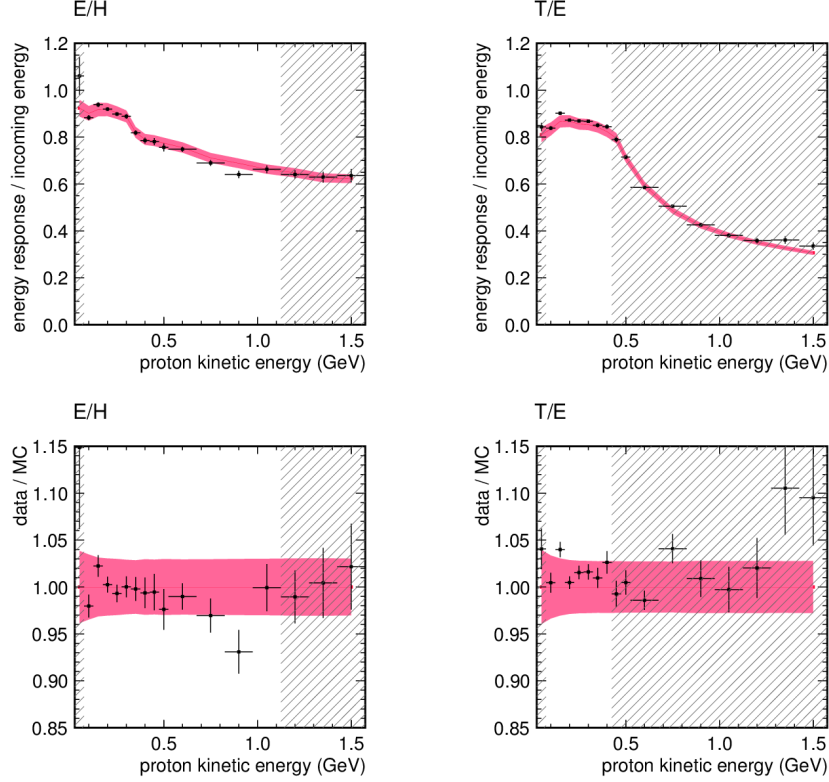


Figure 7: Proton response for EH left and TE right. The bottom plots show the ratio data/MC. The hatched region shows the response in for energies where containment becomes poor. The MC error band includes systematics described in Sec. 7. See text for discussion.

The proton response has several features in this energy range. At low energy, the probability for a proton nuclear interaction is low. The result is there is little missing energy, and also the distribution of response is approximately Gaussian around its mean. At 0.3 GeV, the protons begin to enter the HCAL in the EH detector and begin to produce Δ resonances when they interact in nuclei in

both EH and TE configurations. Both lead to a drop in response, the former as the high dE/dx end of a proton often happens in the steel, the latter because Δ production generically leads to lower response through neutral final states and
445 unbinding of additional nucleons.

The MC tracks the proton response well over the entire range. This is shown in the ratio data/MC for the mean response in each energy bin. The MC has negligible statistical uncertainty; the systematic uncertainty on this ratio is shown as a band on the MC in Fig. 7 and described in detail in Sec. 7. The data
450 is shown with statistical uncertainties. Despite a cut on time of flight applied to data and MC, there may be additional pion background at 0.15 GeV in the proton data because those protons take 19 ns to travel the beamline. This data point, and the data point at 0.9 GeV, stand out especially in the lower figure of Fig. 7. They correspond to no other special features of the experimental setup,
455 and have the character of a $\sim 3\sigma$ fluctuation.

The response at low energy for the TE detector is partly correlated to the tuning of Birks' parameter, because up to 0.25 GeV they are the same proton events. However, the strip response energy scale does not come from the free parameter in the Birks' analysis, which would make this correlation even more
460 complete. Instead, the muon equivalent unit calibration was redone using the measured Birks' parameter to obtain the final strip energy calibration. Thus energy response offsets are correlated only with the Birks' parameter through its uncertainties, and not the overlap of the data events.

In Fig. 7 we show the comparison of data and MC in a region at higher
465 energy, which is shaded. At these energies in the TE configuration we are losing containment of charged particles produced in the hadronic interaction, and the calorimetric response no longer represents the kind of result we expect for the larger MINERvA detector. Instead, these points demonstrate only that the MC is still doing an adequate job describing the data.

470 In addition to the response, it is important for MINERvA neutrino analyses that we know the fluctuations in the response are well simulated. Many neutrino distributions are strongly peaked in reconstructed energy or some other kine-

matic quantity, and an error in resolution will flatten or sharpen the MC peak relative to the data, causing a bias in unfolded distributions and fit parameters.

475 The basic shape of the distribution of response particle-by-particle is well described, so it is adequate to use the RMS of the distribution to quantify the trend and the agreement, as shown in Fig. 8. The statistical uncertainty on the RMS is shown, no systematic uncertainty is quantitatively considered.

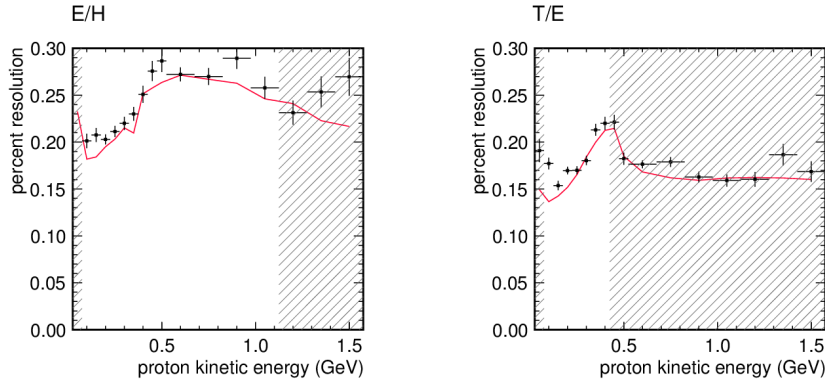


Figure 8: Calorimetric resolution in proton response for the EH configuration (left) and TE (right).

At all energies, the MC response has a lower RMS, more prominent at low
 480 energy. Though the deviation can be taken to be a conservative uncertainty on the calorimetric resolution, a possible explanation for the degraded resolution in data is the addition of beamline induced backgrounds which are not simulated. This is not expected to have the same magnitude effect for higher energy protons, the pion sample, or the same origin as events in the MINERvA detector.

485 The resolution changes from 0.3 to 0.5 GeV because of two effects mentioned previously. This is the region where proton interactions start to produce Δ resonances, responsible also for the decrease in response seen in the upper left plot of Fig. 7. Secondly, in the EH configuration, this is the energy range where protons to reach the HCAL, and the high dE/dx endpoint of the proton is likely
 490 in the steel.

Of special interest is the resolution for the lowest energy protons which are contained in the tracker portion of the TE detector configuration. These correspond to the protons typically found at the vertex of a neutrino interaction from quasi-elastic and resonance production and include products of the intranuclear rescattering process. In the 0.05 to 0.2 GeV range, the resolution is around 17% and the distribution is nearly Gaussian. This range of energy is from protons energetic enough to travel through more than one plane but not energetic enough to excite Δ resonances in the nucleus. The largest contributions to the resolution are from fluctuations at the end of the range and (for data only) from beam-induced background activity. Above this point Δ production becomes important, reducing the stopping component to about half the total. The distribution from which the RMS is computed picks up a low-side tail whose shape is well modeled by the MC.

7. Systematics for single particle response

The systematic uncertainties on the single particle response described in detail here also apply to the pion measurement with only a few differences. It is convenient to present them together here to first complete discussion of the proton measurements, and as a prelude to interpreting the pion measurements in Sec. 8. These systematic uncertainties are evaluated using a variety of methods. Some are done by varying the selection criteria for data and MC and evaluating inconsistencies in the changed response, others are done comparing a modified MC to the default MC, and some are done by dividing the data sample into halves according to natural variations in detector and run conditions. The significant sources of uncertainty are described in Table 2.

7.1. Beam momentum

This uncertainty is intrinsic to the design of the beam and the estimate of the momentum of the incoming particle. An uncertainty here has the trivial effect of shifting the denominator of the fractional response. It comes from

Source	TE p	EH p	EH π^+	EH π^-
Beam momentum	1.9%	1.9%	1.0-2.0%	1.0-2.0%
Birks' parameter	2.0 to 0.9	2.0 to 1.2	1.0	1.0
Correlated late activity	0.3	0.6	1.4	1.4
Temperature stability	1.0	1.0	1.0	1.0
Relative energy scale	0.6	0.6	0.6	0.6
PMT nonlinearity	0.7	0.7	0.9	0.9
Event selection	<0.2	<0.2	0.7	1.5
Cross talk	0.7	0.9	0.5	0.5
Beamline mass model	0.7	0.7	<0.2	<0.2
Total	3.3 to 2.7%	3.4 to 2.9%	2.6 to 3.4%	2.9 to 3.6%

Table 2: Percent systematic uncertainties on the single particle fractional response for data vs. MC comparisons. Additional uncertainties on the energy scale and absorber material apply 2.0% equally to data and MC absolute response, as described in the text. The total range represents the evolution with energy from 0.1 to 0.4 GeV for TE protons, 0.1 to 1.0 GeV for EH protons, and 0.4 to 2.0 GeV for both pion samples.

the wire chamber survey and the measurement and simulation of the magnetic
520 field. Because it is an uncertainty on the momentum, it translates differently to
uncertainties on the available particle energy for protons and pions. The lowest
energy protons pick up an additional 0.7% uncertainty on the energy loss in the
material of the beamline which is included in the total. With this and all other
uncertainties, any energy dependence is included the error band and the total
525 even if not summarized in individual lines in the table.

7.2. Birks' parameter

Even after producing a best fit Birks' parameter, the remaining improved
uncertainty is still one of the largest contributions to the accuracy of the result.
Because low energy protons almost always have a high dE/dx activity at the
530 very end of the proton's range, and because that activity is a larger fraction of
the total energy for low energy protons, that sample is most affected by this

uncertainty. The $\pm 1\sigma$ uncertainty is treated as uncorrelated with the energy scale and non-linearity uncertainties.

7.3. *Correlated late activity*

535 Some systematics are revealed by varying event selection cuts. Proton response, and especially pion response changes when a cut is applied to remove events when additional activity is reconstructed within 800 ns following the triggered event. The response in the MC, which has neither beamline-induced backgrounds nor PMT afterpulsing simulated, is higher because of the correlation with neutrons from the hadronic interaction(s), electrons from π to μ to e decay, and other delayed activity. Systematically, these features follow pions with low fractional energy response. The response for the data is the opposite, it falls slightly and ends about 1% below the MC prediction. Particles removed with this cut in the data due to unrelated beamline activity should
540 be uncorrelated with the energy of the triggered event, and not bias the mean response. Instead, data particles with large shower activity and possibly less missing energy generate more afterpulsing and are more likely to have activity in the 800 ns after the event. If the effect was primarily afterpulsing, this would not be a systematic uncertainty, but an investigation did not confirm that hypothesis. This could be a Geant4 modeling effect, but we have not ruled out an
550 experimental effect, so this is included in the uncertainty.

7.4. *Temperature stability*

The response of the detector to cosmic ray muons for the data is calibrated against the measured temperature in the experimental hall as a function of time.
555 This accounts for the change over the course of the day and from day to day during the run. A correction is then applied to energy deposits in the beam data, while the simulation has no temperature dependence. The uncertainty is evaluated by comparing the response of the high temperature half of the data to the low temperature half.

560 *7.5. Relative energy scale*

The calibration procedure uses a comparison of simulated cosmic ray muons to measured muons, so by construction the data/MC relative energy scale is very well constrained. (The absolute energy scale is limited by our knowledge of the material model for the scintillator planes and affects both data and MC.)
565 The largest contribution to this relative uncertainty comes from observations of discrepancies between the TE and EH data sets. Within each subsample, there is no discernable time dependent trend in the energy response that can be extrapolated between these two detector configuration. The uncertainty listed here is taken to be half the discrepancy seen in the muon calibrations between
570 the TE and EH data sets.

7.6. PMT nonlinearity

A nonlinearity reference curve is available from bench tests of these photo-multiplier tubes, and is a suppression as a function of the total measured charge. Half the reference curve approximately accounts for the translation from bench
575 test conditions to detector conditions. The Birks' parameter measurement yields only an upper bound for the magnitude of this effect, but that result is obscured by correlations with other systematics. We use half the reference curve as the uncertainty here, applied to reduce the reconstructed energy of the MC on a strip-by-strip basis. Nonlinearity is a large effect for rare high activity strips,
580 but for hadronic tracks and showers at these low energies the overall effect is modest. This effect is one way because there is no PMT nonlinearity in the simulation, so it serves only to move the simulated energy lower.

7.7. Event selection

In protons, variations in the event selection do not produce significant uncertainty, even near 0.15 GeV kinetic energy where the 19 ns pileup appears. The
585 pion sample selection intrinsically allows in an electron and kaon background. Variations in those selections yield a 0.7% uncertainty for π^+ and twice the uncertainty for π^- .

7.8. Cross talk

590 A measurement of the optical and electronic cross talk in the cosmic muon calibration finds it contributes an average of $4.2 \pm 0.5\%$ to the energy in the detector, and the amount in the MC is tuned to reproduce this. Because the energy calibration of the detector specifically does not include cross talk, the latter is subtracted from the total, and the remaining 0.5% contributes directly
595 to the calorimetric uncertainty between data and MC. Analysis of neutrino data also has cross talk in the simulation tuned to the data, but uses multiple techniques depending on the analysis to deal with cross talk, including thresholds, topological identification, and subtraction.

7.9. Absolute energy scale

600 There are additional effects which apply equally to both data and MC absolute energy scale. These enhance the absolute uncertainty beyond to the relative energy scale uncertainties. The most important come from the material model for the scintillator planes and also the lead and steel absorber. They affect both the calibration of the energy deposits in the detector as well as how deep the
605 hadronic activity propagates into the detector. They add an additional 2% in quadrature to the quantities in Table 2 for any situation where the absolute uncertainty is needed.

7.10. Geant4 step size

The simulation is affected by a number of different Geant4 settings, including
610 some that are unrelated to the hadronic physics model. A setting of particular interest is the maximum step size allowed by the Geant4 adaptive step size algorithm. Purposely making the maximum step size 0.05 mm allows the adaptive algorithm to still choose smaller steps near material boundaries but never larger steps. This change results in a reduced MC response of 1% for pions and has
615 no effect for 0.5 GeV/c electrons. This is consistent with causing an enhanced Birks' effect because then the simulation produces more highly quenched energy deposits; compare the opposite study in Sec. 5 of 4% enhancement in the last

plane with activity for a more coarse stepping. The baseline simulation uses essentially the default Geant4 settings, the same as used for the rest of the MINERvA experiment, so all the calibrations and measurements are done with a consistent set of parameters, and there is no uncertainty to assign.

8. Pion calorimetry

There are pion samples with two polarities. The EH π^+ sample was obtained concurrently with the proton sample while the π^- sample was from the data set taken the previous week. After these data were taken, the detector configuration was changed to the TE configuration, but unlike for protons, containment in the TE is not adequate for a pion calorimetry measurement. Another difference is that the lowest beam momenta available cause the lowest pion energy for this analysis to be 0.35 GeV, just above the Δ production peak. The mean free path is around 30 ECAL planes, so very few pions stop at the end of their range in the detector, but many reach the HCAL before interacting.

The event selection and energy measurement proceed similar to the proton case, including correcting the observed energy for passive material, cross talk, and the last-four-plane veto. The denominator for the fractional response for pions is taken to be the total energy. For pions there is a potential background at low energy from electron contamination and at high energy from kaons (see Fig. 2) which is neither simulated nor subtracted. Variations in the selection process results in only small changes to the response.

The background due to unrelated activity from the beam has been estimated two ways, by measuring activity 30 ns earlier than the triggered particle and for the lowest energy proton sample by measuring activity deep in the detector where there should be negligible activity. When extrapolating these estimates to the whole detector and time of the event, they both yield the same 4 MeV per event on average. For the mean response, this is simply subtracted before calculating the fractional response. At higher energy, the use of the last-four-plane veto leads to another downward bias of about 1% estimated using the

MC, because real hadron interactions put energy into those planes. This bias is removed with a MC-based energy dependent correction. This procedure is different than is done for protons, but leads also to negligible uncertainty.

650 The MC describes the response to pions imperfectly, and is shown in Fig. 9. The statistical uncertainty on the data is shown while the same for the MC is negligible, and all systematic uncertainties (with their energy dependence) from Table 2 are incorporated into the MC error band. The MC models the single particle response to within 4% up to 1.0 GeV, and 3% up to 2.0 GeV.

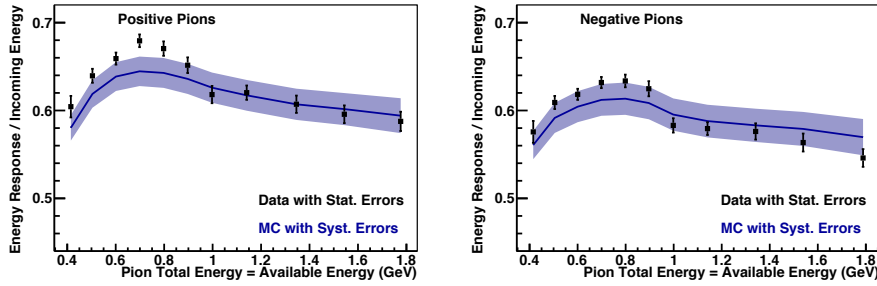


Figure 9: Calorimetric response for positive (left) and negative (right) pions. The errors on the data are statistical only, while the error band on the MC represents the systematic uncertainties on comparisons between data and MC. A larger uncertainty of up to 4.2% (not shown) applies to the absolute response scale both data and MC.

655 This agreement is adequate for MINERvA's neutrino program, sets the uncertainty, and no correction is necessary. However, the MC does not accurately model a change in behavior that starts at 0.9 GeV. This change correlates with a milder inflection point predicted for the MC response. The onset and the magnitude of the discrepancy are the same for both π^+ and π^- , equivalent to
660 a 5% decrease from low to high energy relative to the MC. The experimental systematic uncertainties permit some shape distortion for higher energy relative to low, about equally from the beamline systematics, species selection, and beamline-induced backgrounds. When evaluated in quadrature, these could produce a $\pm 1.8\%$ relative change over this energy range, less than half what
665 is observed. None of these systematics would naturally produce a change over

a short 0.2 GeV energy range near 0.9 GeV. Instead of taking an overall uncertainty in the response, a MINERvA neutrino analysis sensitive to this will propagate the trend.

In principle, these data are a test of our ability to model the detector itself
670 but also the pion energy loss and reaction processes such as inelastic, absorption, charge exchange, and elastic scattering. We have investigated the sensitivity to model uncertainties using the Bertini Cascade model [14] within Geant4, including consideration of pion cross section data [15, 16]. However, calorimetry is more sensitive to the total available energy than it is to differences in outcome for any of these individual fates. Trial 30% modifications to the relative
675 mix of fates have at most a 0.5% effect on calorimetry. Instead, increasing the probability to interact (inelastic or elastic with at least 10 MeV energy transfer) before reaching the HCAL enhances the response. By this definition of interaction, the mean free path in the ECAL is about 30 planes; lowering it by 20%
680 increases the calorimetric response by 1.5%.

Uncertainties on the models in Geant4 in principle could be energy dependent, so a tuned model could better describe the overall average response or separately the anomalous trend with energy. An investigation of the trend reveals a correlation with the fraction of events that have negligible energy in
685 the HCAL: the MC does not follow the data and underestimates this fraction starting at 0.9 GeV. This is also a predicted effect of a too-low mean free path but detailed comparisons of the lateral and longitude distribution of energy are beyond the scope of this result. Simple followup investigations do not corroborate this mean free path hypothesis. Further analysis may be possible, including
690 followup data being taken now. Though no experimental systematic by itself is expected to have these features, we do not rule out an artifact of the experimental setup or analysis.

The ratio of detector response to positive pions over detector response to negative pions cancels a number of common systematics and the trends described
695 in the preceding paragraphs. The MC predicts that π^+ yield a 4.8% higher

response than π^- . The measured ratio is 6.2%, with no energy dependence for either data or MC. The statistical uncertainty in the ratio in data is only 0.5% averaged over all energies. another 0.6% uncertainty in the data/MC relative energy scale comes primarily from the unknown time or detector configuration dependent effect described in Sec. 7, which should conservatively be applied to interpret this ratio. There is no evidence for either an intensity effect (the π^+ data was at higher intensity), or an operational effect due to time or polarity in the beamline, nor a temperature effect. These are judged by comparing two halves of each data configuration further split along these operational parameters, though these tests are themselves afflicted by 0.7% statistical uncertainty. This 6.2 - 4.8 = 1.4% discrepancy is at two standard deviations, and it can be used as a conservative uncertainty on the ratio, when applying it to neutrino analyses.

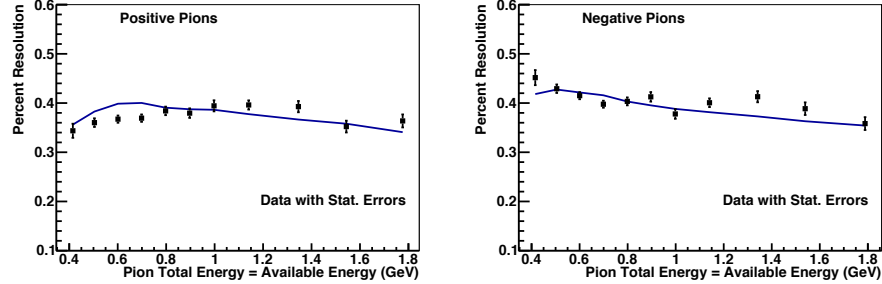


Figure 10: Resolution of the calorimetric response for positive (left) and negative (right) pions. The statistical error on the RMS is shown for the data, no systematic uncertainties are included.

As with the proton case, Fig. 10 shows the pion fractional response resolution is adequately modeled. The beam-induced backgrounds are a much smaller fraction of the total energy than for low energy protons, the Δ production peak happens at energies below these, and a large fraction of the events reach the HCAL, so there is none of the structure seen in the proton case.

9. Electron calorimetry

715 The electron sample is limited to energies in a range from 0.4 to 0.5 GeV. The production of electrons is intrinsically lower in energy and fewer than pions, and the TOF resolution prevents good identification of the few that are at higher energies. In the EH detector configuration, electrons in this energy range deposit 95% or more of their energy in the ECAL portion of the detector, and the
720 response of the ECAL alone can be measured. The TE detector configuration is similar: the electron propagates through the tracker but does not shower extensively until the ECAL.

The electron sample is separated from the pion sample using a combination of topological and time-of-flight selections. Events that resemble late-interacting
725 pions because they are tracked into the HCAL or because they have a substantial fraction of energy in the back half of the detector are rejected. Further, the number of strips recording activity is systematically more for electrons, and the variance in energy per plane for EM showers is much higher than for interacting pions. Using the MC, we estimate the efficiency for selecting electrons (pions)
730 to be 61% (5%) for the TE and 73% (8%) for the EH configuration. The pion and electron peaks separate in time of flight by at least 0.7 ns at 0.5 GeV, well within the 0.2 ns resolution of the TOF. Extrapolating the pion distribution just above the TOF cut into the selected electron region in data yields an estimate of one pion background in 50 electron events. An eye-scan of the resulting events
735 with the web-based MINERvA event display [7] yields one obvious background event which is removed, leaving 49 events total in the EH sample.

The resulting sample is analyzed similarly as previously described for protons and pions. The data and MC for electrons and positrons for the EH configuration were combined into one sample. After correcting for passive material,
740 cross-talk, and beamline-induced background activity, the response ratio is obtained for every event. The electron fractional response is found to be 0.763 ± 0.013 (statistical) in data and 0.740 ± 0.002 (statistical) in MC. There is an additional 1.9% relative systematic uncertainty between the data and MC,

bringing the total uncertainty to 2.6%. Further adding uncertainties from the
745 material assay brings this to 3.2% absolute uncertainty. The data response is 3%
higher than the MC predicts, a little more than the total relative uncertainty.
The MC predicts a resolution of 11.5%, which is an adequate description of the
low statistics data.

The MC predicts the response in the TE configuration is 3% higher than the
750 EH configuration because most electrons ionize their way through the tracker
before electromagnetic showers develop in the ECAL. This sample provides an-
other 62 events, more of them are positrons than electrons because of the running
conditions. Again a 3% discrepancy response is seen in these TE results, as with
the EH results. The systematic uncertainty is somewhat larger but the statis-
755 tical uncertainty is smaller, because of slightly better statistics and resolution.
The data/MC relative total uncertainty is 2.4%, and the absolute uncertainty
on the response is 3.1%. The MC prediction of a 9.1% resolution describes the
data well.

This sample is subject to the same systematics as the proton and pion results
760 plus additional 1.1% uncertainty due to the electron-pure selection. Comparing
the default MC to a variation with $\pm 1.2\%$ Pb density in the ECAL reveals only
a $\pm 0.15\%$ change in response for the TE configuration and $\pm 0.3\%$ change for
the EH sample. Variations of the event selection contributes 1% uncertainty
to the response. The absolute energy scale uncertainty is the same 2% and
765 the data vs. MC relative uncertainty is 0.7% from the material model effects
and calibrations described previously. Another 0.5% comes from the cross talk
model. Finally, the beam momentum uncertainty is 1% at these energies.

For high energy hadronic showers, it is traditional to quote the e/π response
ratio. A shower initiated by a charged hadron may have both hadronic and elec-
770 tromagnetic components, the relative fractions of which evolve with energy and
vary stochastically event-by-event. An e/π response calibration constrains the
relative accuracy of these response components. In this detector, the compari-
son of the higher 0.8 for electrons to the lower 0.6 response for pions provides a
helpful estimate.

775 10. Calorimetry discussion

In addition to the classic and exhaustive monograph on high energy calorimetry by Richard Wigmans [17], there are several recent test beam measurements using segmented scintillator and absorber calorimeters and hadron simulations similar to ours.

780 The MINOS neutrino experiment uses a detector made of scintillator and inch-thick iron, very similar to the MINERvA HCAL. Their test beam exposure in the CERN T7 and T11 beamlines was analyzed to produce electron [18] and hadron [19] calorimetry results. They compared their data to a GEANT3 simulation and found several discrepancies at the 3% to 6% level. However, 785 our data are compared to a Geant4 simulation, so comparison to the present analysis is indirect.

The CALICE experiment has data from operating several kinds of sampling calorimeters in beams at Fermilab and CERN. They use similar, Geant4 based hadron and electromagnetic models, but their data is mostly at higher energy. 790 The analysis of their data is ongoing. As of this writing, two publications [20, 21] make for good comparison to the MINERvA test beam data.

Hadronic calorimetry is considered [20] for data taken with an iron-scintillator calorimeter. They find Geant4 models underestimate the measured response by 3% at 8 GeV/c momentum their lowest pion data available. This is beyond the 795 edge of their 2% uncertainty. This is also the only data point in their many model comparisons where Geant4 is using the same Bertini cascade model used in our simulation, shown in the lowest (blue) line in the lower left plot in their Fig. 6. Their data show a trend with energy such that the MC overestimates the data above 20 GeV or so, but remain consistent within their uncertainty 800 estimates.

In the later paper [21], data from a tungsten segmented calorimeter is compared to Geant4 models for electrons, pions, and protons. The π^+ response for the same Bertini cascade model (but from Geant4 9.6.p2) describes their mean response very well from 3 to 8 GeV. The discrepancy is less than 2% while their

uncertainty is around 3%. These are the same models with data at some of the same energies, but using data from a different detector and beam compared to the iron calorimeter in [20]. Agreement also follows for proton data in the same range. A similar result is obtained for positrons, agreement above 2 GeV. However, the simulation underestimates the data by 2.5% at 1 GeV, just within 1σ agreement for the lowest positron energy for which they have data.

Taken together, the MINERvA and CALICE data suggest that the Bertini cascade model from recent (9.4p2 and later) Geant4 does a good job of describing hadronic data at the 4% level in an iron-scintillator calorimeter through the combined range of energy. CALICE indicates that the electromagnetic cascade model applied to an ECAL style calorimeter also does very well. But the low energy data point that is similar to MINERvA's suggests the MC underestimates the response in both cases.

A final, general comment: hadron calorimetry at energies below 2 GeV follows a process where one hadron undergoes zero or one inelastic interaction, with a small number of outgoing particles. It is not easily characterized by the statistical \sqrt{E} and \sqrt{N} effects typical of hadron calorimetry at higher energies.

11. Tracking validation

The proton sample in the TE detector configuration allows us to validate proton tracking efficiency: the probability that a proton will be reconstructed as a three-dimensional track object. The proton tracking efficiency, and that for pions, is important for measurements of neutrino differential cross sections with specific proton and pion final states.

The sample is similar to the one used for the Birks' parameter measurement where protons stop no later than plane 19, but without the requirement that its depth be consistent with a proton at the end of its range. Another difference, the sample is extended to protons whose last activity is only as far as plane six. This tests a combination of the standard MINERvA "long tracker" which requires a minimum of eleven planes and two variations of the short tracker

which can form tracks with as few as five planes of activity. For this analysis,
835 the MC sample is four times the size of the data sample.

The efficiency for long tracks is nearly perfect. Specifically the sample of protons with kinetic energy less than 0.4 GeV whose last energy deposit is between planes nine and nineteen (inclusive) are tracked with efficiency of $99.2^{+0.2}_{-0.3}\%$ in data and $99.8\pm0.1\%$ in MC. For the data, this corresponds to tracking 1520 out
840 of 1533 protons in the sample. Around 60% of protons stop a distance consistent with the end of their range, and failing the tracking is highly correlated with a proton experiencing an interaction.

Differences begin to appear for even shorter proton samples. For the 185 protons that appear to stop in plane eight, 178 of them were tracked, which gives
845 $96.2^{+1.2}_{-1.6}\%$ compared to the MC $97.7^{+0.5}_{-0.6}\%$. For 338 protons that appear to stop in planes six and seven only 308 are tracked, $91.1^{+1.5}_{-1.6}\%$ compared to the MC $96.5\pm0.5\%$. These subsamples have a 70% fraction with their stopping location at the end of their expected range. It is more likely in the data that a short event at the end of its expected range will not pass the tracking requirements.

850 The above results for protons were obtained with a short tracker configured for a neutrino pion production analysis [5]. A somewhat different configuration optimized for a quasi-elastic proton analysis [6] gives 1 to 2% higher efficiency, successfully tracking an additional 6, 1, and 8 events in the data subsamples for the shortest, 8-plane, and longest samples respectively, with a similar trend of
855 better tracking in the MC. The results from the test beam data are then applied to both proton and pion tracking in the neutrino analyses.

The main reason for the difference between the two tracking techniques involves the choice of candidate clusters of activity to give to the tracking algorithm. The QE-proton algorithm is more permissive, especially allowing clusters
860 with more hits and more energy that would be expected from a simply ionizing particle. The pion tuned algorithm excludes these when deciding whether to form a track. In the case of very short, six-plane tracks, excluding one plane has a large effect.

These results suggest that tracking efficiency is adequately modeled (within

1%) for tracks greater than 9 planes, which makes it a negligible uncertainty for neutrino analyses. In contrast, we can use a data-based correction of as much as 5% to the efficiency for shorter track lengths, relative to the MC predicted efficiency. The tracking algorithm also has to deal with activity near the neutrino interaction point and wider range of angles relative to the detector axis, which are not addressed by the test beam sample. Therefore, this efficiency correction should be on top of the MC prediction for efficiency that considers other effects seen in real neutrino interactions.

12. Conclusion

We have measured the performance of the tracking and calorimetry of the MINERvA detector design by exposing a scaled-down version of the detector to a test beam of low momentum protons, pions, and electrons from the Fermilab Test Beam Facility. These data provide a constraint on the Birks' law saturation effect for our formulation of polystyrene based plastic scintillator. The calorimetric response to protons and pions within the range of energies tested yields uncertainties of 4% when the single particle calorimetric response is used in neutrino analyses. There are several effects that could be interpreted as 2σ fluctuations relative to the systematic uncertainties, but overall the MC describes the data and its resolutions well. The electron sample yields a similar uncertainty. Tracking performance is well modeled, and we have measured a small discrepancy between the performance of tracking in the data and simulation.

References

- [1] L. Aliaga, et al., Design, Calibration, and Performance of the MINERvA Detector, Nucl.Instrum.Meth. A743 (2014) 130–159. [arXiv:1305.5199](#), [doi:10.1016/j.nima.2013.12.053](#).
- [2] L. Fields, J. Chvojka, et al., Measurement of Muon Antineutrino Quasi-Elastic Scattering on a Hydrocarbon Target at $E_\nu \sim 3.5$ GeV, Phys. Rev.

- Lett. 111, 022501. `arXiv:1305.2234`, `doi:10.1103/PhysRevLett.111.022501`.
- [3] G. Fiorentini, D. Schmitz, P. Rodriguez, et al., Measurement of Muon
 895 Neutrino Quasi-Elastic Scattering on a Hydrocarbon Target at $E_\nu \sim 3.5$
 GeV, Phys. Rev. Lett. 111, 022502. `arXiv:1305.2243`, `doi:10.1103/PhysRevLett.111.022502`.
- [4] B. Tice, M. Datta, J. Mousseau, et al., Measurement Ratios of ν_μ Charged-
 900 Current Cross Sections on C, Fe, and Pb to CH at Neutrino Energies 2-
 20 GeV, Phys. Rev. Lett. 112, 231801. `arXiv:1403.2103`, `doi:10.1103/PhysRevLett.112.231801`.
- [5] B. Eberly, et al., Charged Pion Production in ν_μ Interactions on Hydro-
 carbon at $\langle E_\nu \rangle = 4.0$ GeV `arXiv:1406.6415`.
- [6] T. Walton, M. Betancourt, et al., Measurement of muon plus proton final
 905 states in ν_μ Interactions on Hydrocarbon at $\langle E_\nu \rangle = 4.2$ GeV `arXiv:1409.4497`.
- [7] N. Tagg, et al., Arachne - A web-based event viewer for MINERvA,
 Nucl.Instrum.Meth. 676 (2012) 44–49. `arXiv:1111.5315`, `doi:10.1016/j.nima.2012.01.059`.
- 910 [8] S. Agostinelli, et al., GEANT4: A Simulation toolkit, Nucl.Instrum.Meth.
 A506 (2003) 250–303. `doi:10.1016/S0168-9002(03)01368-8`.
- [9] J. Allison, K. Amako, J. Apostolakis, H. Araujo, P. Dubois, et al., Geant4
 developments and applications, IEEE Trans.Nucl.Sci. 53 (2006) 270. `doi:10.1109/TNS.2006.869826`.
- 915 [10] J. B. Birks, , Proc.Phys.Soc. A64 (1951) 874.
- [11] J. B. Birks, The Theory and Practice of Scintillation Counting.

- [12] V. Tretyak, Semi-empirical calculation of quenching factors for ions in scintillators, *Astropart.Phys.* 33 (2010) 40–53. [arXiv:0911.3041](#), [doi:10.1016/j.astropartphys.2009.11.002](#).
- 920 [13] L. Reichhart, D. Y. Akimov, H. Araujo, E. Barnes, V. Belov, et al., Quenching Factor for Low Energy Nuclear Recoils in a Plastic Scintillator, *Phys.Rev. C*85 (2012) 065801. [arXiv:1111.2248](#), [doi:10.1103/PhysRevC.85.065801](#).
- 925 [14] A. Heikkinen, N. Stepanov, J. P. Wellisch, Bertini intranuclear cascade implementation in GEANT4, eConf C0303241 (2003) MOMT008. [arXiv:nucl-th/0306008](#).
- [15] D. Ashery, I. Navon, G. Azuelos, H. Walter, H. Pfeiffer, et al., True Absorption and Scattering of Pions on Nuclei, *Phys.Rev. C*23 (1981) 2173–2185. [doi:10.1103/PhysRevC.23.2173](#).
- 930 [16] B. Allardyce, C. Batty, D. Baugh, E. Friedman, G. Heymann, et al., Pion reaction cross-sections and nuclear sizes, *Nucl.Phys. A*209 (1973) 1–51. [doi:10.1016/0375-9474\(73\)90049-3](#).
- [17] R. Wigmans, *Calorimetry: Energy Measurement in Particle Physics*, *Int.Ser.Monogr.Phys.* 107 (2000) 1–726.
- 935 [18] P. L. Vahle, Electromagnetic interactions in the MINOS detectors (Ph.D thesis 2004).
- [19] M. A. Kordosky, Hadronic interactions in the MINOS detectors (Ph.D. thesis 2004).
- 940 [20] C. Adloff, et al., Validation of GEANT4 Monte Carlo Models with a Highly Granular Scintillator-Steel Hadron Calorimeter, *JINST* 8 (2013) 07005. [arXiv:1306.3037](#), [doi:10.1088/1748-0221/8/07/P07005](#).
- [21] C. Adloff, J. J. Blaising, M. Chefdeville, C. Drancourt, R. Gaglione, et al., Shower development of particles with momenta from 1 to 10 GeV in the

CALICE Scintillator-Tungsten HCAL, JINST 9 (2014) P01004. [arXiv:](#)

945

1311.3505, [doi:10.1088/1748-0221/9/01/P01004](#).